B. Power System Model

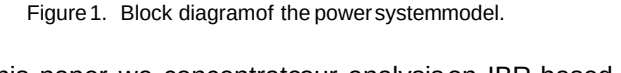

Figure 1. Block diagram of the power system model.

In this paper, we concentrate our analysis on IBR-based power systems[1]. We consider a (connected) network-reduced power system consisting of buses indexed by $\mathcal{V} := \{1, \dots, N\}$, where N denotes the number of IBRs in the network, with the block diagram structure given in Fig. 1. Without loss of generality, we assume that the first node provides an angle reference to the rest of the network. We denote each transmission line by the unordered pair $(j, k) \in \mathcal{E}$. We define the following:

$$\text{vec}\begin{bmatrix} P_i \\ Q_i \end{bmatrix}_{i\in\mathcal{V}} = [P_1, Q_1, \dots, P_N, Q_N]^T.$$

We use similar definitions for $\text{vec}\{[d_{P,i}, d_{Q,i}]^T\}_{i\in\mathcal{V}}\}$, $\text{vec}\{[P_i^0, Q_i^0]^T\}_{i\in\mathcal{V}}\}$, and $\text{vec}\{[\dot{\theta}_i, V_i]^T\}_{i\in\mathcal{V}}\}$.

The closed-loop system is modeled as the feedback interconnection of bus dynamics $H(s)$ and the linearized network model $\frac{1}{s}L_B$. For the i-th bus, the exogenous signals $[P_i^0, Q_i^0]^T \in \mathbb{R}^{2\times 1}$ and $[d_{P,i}, d_{Q,i}]^T \in \mathbb{R}^{2\times 1}$ respectively represent the power injection setpoint and power fluctuations around the setpoint that indicates, for example, variations in power drawn by local loads. The output signals $[\dot{\theta}_i, V_i]^T \in \mathbb{R}^{2\times 1}$ represent the bus frequency and voltage derivative, respectively. Through the network, the signals $[\dot{\theta}_i, V_i]^T$ are mapped to the power demand $[P_i, Q_i]^T$. Furthermore we make the following assumptions for the power system model. First, transmission lines are lossless. Second, at equilibrium, the angle difference across each transmission line is less than 90°. These assumptions are well-justified and generally hold for most transmission systems [13]. In addition, we use $V_{\max,0j}$ to represent the maximum per unit steady state voltage magnitude of bus j. We denote the maximum steady state voltage among all buses j neighboring bus i as $\max_{j\in\mathcal{N}_i}\{V_{0j}\}$.

We now discuss the model of the different components in the system in more detail.

1) Bus dynamics: In this paper, we work with droop-based GFM inverters. The dynamics are composed of the droop-based control laws described by [6], [14],

$$\begin{cases} \dot{\theta}_i = \omega_i \\ \omega_i = \omega_i^0 + m_i^p f_i^p(s)((P_i^0 + d_{P,i}) - P_i), & \forall i \in \mathcal{V}, \\ V_i = V_i^0 + m_i^q f_i^q(s)((Q_i^0 + d_{Q,i}) - Q_i), \end{cases} \quad (1)$$

where $m_i^p \in \mathbb{R}_{>0}$ and $m_i^q \in \mathbb{R}_{>0}$ are the droop gains, ω_i^0 and V_i^0 are the frequency and voltage setpoints, P_i^0, and Q_i^0 are the power setpoints, $f_i^p(s) = \frac{\tau_i^p}{\tau_i^p s+1}$ and $f_i^q(s) = \frac{\tau_i^q}{\tau_i^q s+1}$ represent the low-pass filters applied to the power measurements with DC gains $\tau_i^p \in \mathbb{R}_{>0}$ and $\tau_i^q \in \mathbb{R}_{>0}$, and time constants $\tau_i^q \in \mathbb{R}_{>0}$ and $\tau_i^p \in \mathbb{R}_{>0}$. Substituting in the expression of low-pass filters, we get

$$\omega_i = \omega_i^0 + \frac{m_i^p \tau_i^p}{\tau_i^p s + 1}((P_i^0 + d_{P,i}) - P_i) \quad (2)$$

$$V_i = V_i^0 + \frac{m_i^q \tau_i^q s}{m_i^q s + 1}((Q_i^0 + d_{Q,i}) - Q_i) \quad (3)$$

which respectively give the following transfer functions of frequency and voltage dynamics:

$$h_i(s) = \frac{m_i^p \tau_i^p}{\tau_i^p s + 1}; \quad (4)$$

$$h_i^V(s) = \frac{m_i^q \tau_i^q s}{\tau_i^q s + 1}. \quad (5)$$

The term $m_i^p \tau_i^p$ and $m_i^q \tau_i^q$ represent the effective droop gains. Furthermore, the matrix of bus dynamics $H(s)$ is modeled as

$$H(s) = \text{diag}\{\text{diag}(h_i(s), h_i^V(s))\}_{i\in\mathcal{V}}. \quad (6)$$

Remark 1. The chosen GFM inverter model (1) is relatively simplified because we intend to capture important system-level dynamics. For future studies involving more detailed inverter modeling, for example, incorporating lower-level control loops and integrating various other devices into a multi-machine multi-inverter system, we anticipate dynamic coupling between voltage magnitude V and angle θ in the bus dynamics. This coupling is expected to result in a multi-input-multi-output (MIMO) non-diagonal matrix H.

2) Network model: We consider linearized decoupled power flow equations. This is under the assumption of a lossless network with small angle differences in steady state, which results in very weak coupling between P-V, as well as Q-θ. It is important to note that this assumption may not hold in scenarios such as a low voltage distribution system with a high R/X ratio or in a microgrid. The network model is given by,

$$\text{vec}\begin{bmatrix} P_i \\ Q_i \end{bmatrix}_{i\in\mathcal{V}} = \frac{1}{s}L_B \,\text{vec}\begin{bmatrix} \dot{\theta}_i \\ V_i \end{bmatrix}_{i\in\mathcal{V}} \quad (7)$$

where

$$L_B = \begin{bmatrix} P_{\theta;11} & 0 & \cdots & P_{\theta;1N} & 0 \\ 0 & Q_{v;11} & \cdots & 0 & Q_{v;1N} \\ \vdots & \vdots & \ddots & \vdots & \vdots \\ P_{\theta;N1} & 0 & \cdots & P_{\theta;NN} & 0 \\ 0 & Q_{v;N1} & \cdots & 0 & Q_{v;NN} \end{bmatrix} \in \mathbb{R}^{2N\times 2N};$$

[1] Although the results can be generalized to encompass a mix of synchronous machines and various types of IBRs, we restrict to the homogeneous IBR-based systems due to space limitation.

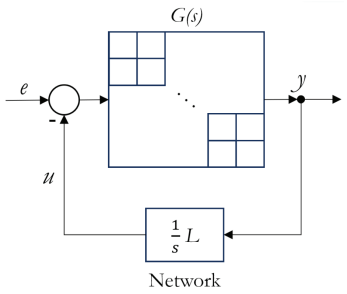

Figure 2. General feedback interconnection.

and

$$\tilde{P}_{\theta,ij} = \frac{\partial}{\partial \theta_j} \sum_{l\in\mathcal{N}_i} -V_i V_l B_{il} \sin(\theta_i - \theta_l)\Big|_{\substack{\theta=\theta_0\\V=V_0}}$$
$$= \begin{cases} -\sum_{l\in\mathcal{N}_i} V_{0i}V_{0l}B_{il}\cos(\theta_{0i}-\theta_{0l}), & i=j,\\ V_{0i}V_{0j}B_{ij}\cos(\theta_{0i}-\theta_{0j}), & i\neq j,\end{cases}$$
$$\tilde{Q}_{V,ij} = \frac{\partial}{\partial V_j}\left(V_i^2 B_{ii} + \sum_{l\in\mathcal{N}_i} V_i V_l B_{il}\cos(\theta_i-\theta_l)\right)\Big|_{\substack{\theta=\theta_0\\V=V_0}}$$
$$= \begin{cases} 2V_{0i}B_{ii} + \sum_{l\in\mathcal{N}_i} V_{0l}B_{il}\cos(\theta_{0i}-\theta_{0l}), & i=j,\\ V_{0i}B_{ij}\cos(\theta_{0i}-\theta_{0j}), & i\neq j.\end{cases} \tag{8}$$

In these equations, $V_0 \in \mathbb{R}^N$ and $\theta_0 \in \mathbb{R}^N$ denote the voltage magnitudes and angles at the buses in steady state. The term $B_{ik} \leq 0$ $(\forall i \neq k)$ denotes the mutual susceptance of the transmission line connecting buses i and k, $B_{ik} = 0$ if there is no line, and $B_{ii} = -\sum_{k\in\mathcal{N}_i} B_{ik} \geq 0$ denotes the self susceptance of bus i.

III. Main Results

In this section, we develop the main decentralized stability criteria for GFM IBR-based power systems. Note that this result can be extended to more general scenarios in multi-machine multi-inverter systems. Due to the space limitation, we defer the discussion of such cases in future work.

We build on a decentralized stability result [12, Th. 1], which is replicated below in **Theorem 1**. The theorem is applicable to a general feedback interconnection as in Fig. 2 with single-input-single-output (SISO) bus dynamics (therefore diagonal matrix $G(s)$) and network model $\frac{1}{s}L$. The system equations are described by,

$$\begin{aligned} y_i(s) &= g_i(s)(e_i(s) - u_i(s)),\\ u(s) &= \tfrac{1}{s} L y(s).\end{aligned} \tag{9}$$

Theorem 1. *[12, Th. 1] Let PR and ESPR denote the set of positive real and extended strictly positive real functions, respectively. If there exists a function $f(s) \in PR \cap \mathscr{A}_0$ where for all bus dynamics it holds that $g(s) \in \mathcal{G}_f$, where*

$$\mathcal{G}_f := \{g(s) \in \mathscr{H}_\infty : g(0) \neq 0,\ f(s)\left(1 + \frac{g(s)}{s}\right) \in ESPR\},$$

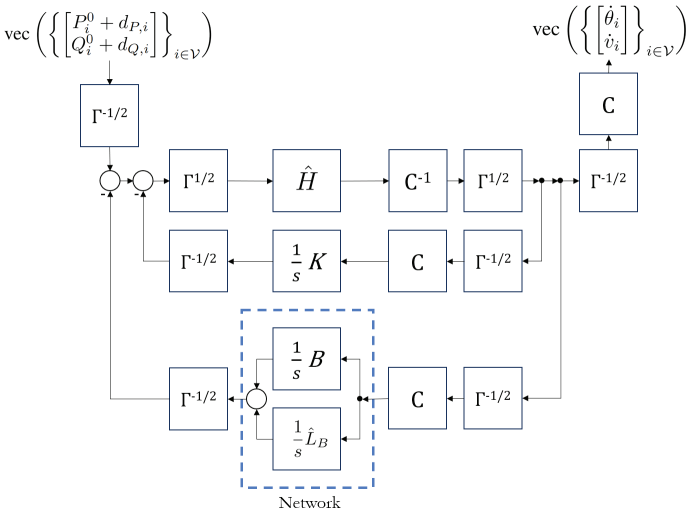

Figure 3. Equivalent system to Fig. 1 unto loop transformation.

then the feedback interconnection in (9) is stable for any network model $L \in \mathcal{L}$, where

$$\mathcal{L} := \{L : L = L^T, 0 \preceq L \preceq I\}.$$

Remark 2. *The key strengths of **Theorem 1** include its capability to handle cases when components are added or removed from the network, and when the operating point changes [12].*

A. Application to IBR-Based Power Systems

We observe that the dynamics of voltage angle and magnitude in (6) are completely decoupled. Consequently, we can treat our model of interest as having separate SISO dynamics, allowing us to utilize the result from **Theorem 1** to formulate the decentralized stability criteria. The key challenge that prevents the application of **Theorem 1** to the power system configuration in Fig. 1 lies in that L_B is not necessarily in $\mathcal{L}$. In this section, we address this challenge by performing loop transformation. We define the following terms,

$$\begin{aligned} \hat{h}_i^V(s) &:= m_i^q \beta_i^q / \tau_i^q,\\ k_i &:= 1/m_i^q\beta_i^q,\\ \gamma_i^p &:= 2\sum_{j\in\mathcal{N}_i} V_{\max,0i}V_{\max,0j}B_{ij},\\ \gamma_i^q &:= k_i V_{\max,0i} + 2V_{\max,0i}^2 B_{ii},\\ \hat{H}(s) &:= \mathrm{diag}(\{\mathrm{diag}(h_i^\theta(s), \hat{h}_i^V(s))\}_{i\in\mathcal{V}}),\\ K &:= \mathrm{diag}(0,k_1,0,k_2,\ldots,0,k_N),\\ \Gamma &:= \mathrm{diag}(\gamma_1^p,\gamma_1^q,\gamma_2^p,\gamma_2^q,\ldots,\gamma_N^p,\gamma_N^q),\\ C &:= \mathrm{diag}(1,V_{01},1,V_{02},\ldots,1,V_{0N}),\\ B &:= \mathrm{diag}(0,2V_{01}B_{11},0,2V_{02}B_{22},\ldots,0,2V_{0N}B_{NN}),\\ \hat{L}_B &:= L_B - B.\end{aligned} \tag{10}$$

It can be shown that the block diagram in Fig. 1 can be transformed equivalently into Fig. 3, with the corresponding terms defined above. Upon combining the two feedback

branches in Fig. 3, we obtain that the corresponding $G(s)$ and L in Fig. 2 are defined by

$$\begin{aligned} G(s) &= \Gamma^{1/2} C^{-1} \hat{H}(s) \Gamma^{1/2}, \\ L &= \Gamma^{-1/2}((K+B) + \hat{L}_B) C \Gamma^{-1/2}. \end{aligned} \tag{11}$$

Next, we show that, facilitated by the loop transformation, the resulting L in (11) can be made to satisfy $0 \preceq L \preceq I$.

Lemma 1. *If for all buses $i \in \mathcal{V}$ it holds that*

$$\left(\max_{j \in \mathcal{N}_i}\{V_{0j}\} - V_{0i}\right) \beta_i^q \leq \frac{1}{2m_i^q |B_{ii}|}, \tag{12}$$

then L as given by (11) satisfies $0 \preceq L \preceq I$.

Proof. By definition in (11), L is symmetric. As a consequence of Gershgorin's Circle Theorem [15], the eigenvalues of matrix $L := \{l_{ij}\}$ live in a ball centered at l_{ii} of radius $\sum_{j \in \mathcal{N}_i} l_{ij}$. Let $\pi : \{1, \ldots, N\} \longrightarrow \{1, \ldots, N\}$ be a bijection. Then every odd row i in L satisfies

$$\begin{aligned} \lambda_{\pi(i)}(L) &\geq l_{ii} - \sum_{j \in \mathcal{N}_i} |l_{ij}| \\ &= \frac{1}{\gamma_i^p} \sum_{j \in \mathcal{N}_i} |V_{0i} V_{0j} B_{ij} \cos(\theta_{0i} - \theta_{0j})| \\ &\quad - \sum_{j \in \mathcal{N}_i} \left| \frac{1}{\gamma_i^p} V_{0i} V_{0j} B_{ij} \cos(\theta_{0i} - \theta_{0j}) \right| = 0. \end{aligned} \tag{13}$$

For every even row i, Gershgorin's Circle Theorem gives

$$\begin{aligned} \lambda_{\pi(i)}(L) \geq & l_{ii} - \sum_{j \in \mathcal{N}_i} |l_{ij}| \geq \frac{1}{\gamma_i^q} k_i V_{0i} + \frac{2}{\gamma_i^q} V_{0i}^2 B_{ii} \\ & + \frac{1}{\gamma_i^q} \sum_{j \in \mathcal{N}_i} V_{0i} V_{0j} B_{ij} \cos(\theta_{0i} - \theta_{0j}) \\ & - \sum_{j \in \mathcal{N}_i} |\frac{1}{\gamma_i^q} V_{0i} V_{0j} B_{ij} \cos(\theta_{0i} - \theta_{0j})|. \end{aligned} \tag{14}$$

Now, suppose the voltage magnitude at each bus j neighboring bus i satisfies (12). Then,

$$\begin{aligned} k_i &\geq 2 \left(\max_{j \in \mathcal{N}_i}\{V_{0j}\} - V_{0i}\right) |B_{ii}| \\ &\geq 2 \sum_{j \in \mathcal{N}_i} \max_{j \in \mathcal{N}_i}\{V_{0j}\} |B_{ij}| - 2 V_{0i} |B_{ii}|. \end{aligned} \tag{15}$$

Since $\frac{1}{\gamma_i^q} V_{0i} \geq 0$, (15) ensures $\lambda_{\pi(i)} \geq 0$ for all even i in (14). Therefore, L is positive semi-definite, or $L \succeq 0$, as a direct consequence of (13), (14), and (15).

Furthermore, we want to prove that it holds that $L \preceq I$ with a similar reasoning. For every odd row i, Gershgorin's Circle Theorem gives $\lambda_{\pi(i)}(I - L)$ satisfies

$$\begin{aligned} \lambda_{\pi(i)}(I - L) &\geq (1 - l_{ii}) - \sum_{j \in \mathcal{N}_i} |l_{ij}| \\ &= 1 - \frac{2}{\gamma_i^p} \sum_{j \in \mathcal{N}_i} |V_{0i} V_{0j} B_{ij} \cos(\theta_{0i} - \theta_{0j})| \\ &\geq 0. \end{aligned} \tag{16}$$

For every even row i, Gershgorin's Circle Theorem gives

$$\begin{aligned} \lambda_{\pi(i)}(I - L) &\geq (1 - l_{ii}) - \sum_{j \in \mathcal{N}_i} |l_{ij}| \\ &= 1 - \frac{1}{\gamma_i^q} \left(k_i V_{0i} + 2 V_{0i}^2 B_{ii}\right) \\ &\geq 0. \end{aligned} \tag{17}$$

Thus, (16) and (17) imply $I - L \succeq 0$ or, equivalently, $I \succeq L$. Therefore, satisfying (12) implies $0 \preceq L \preceq I$. □

B. Decentralized Stability Criteria for IBR-Based Systems

Combining the results in **Theorem 1** and **Lemma 1**, we derive the final result on decentralized stability criteria for droop-controlled IBR-based power systems.

Theorem 2. *Given the feedback interconnection in Fig. 1 consisting of droop-controlled IBRs whose dynamics are given in* (1)*, with the droop constants $m^p \in \mathbb{R}_{\geq 0}$, $m_i^q \in \mathbb{R}_{\geq 0}$ and the filter time constants $\tau^p{}_i$, $\tau_i^q \in \mathbb{R}_{>0}$. The grid-forming IBR-based power system is stable whenever each controller gain satisfies,*

$$\left(\max_{j \in \mathcal{N}_i}\{V_{0j}\} - V_{0i}\right) \beta_i^q \leq \frac{1}{2m_i^q |B_{ii}|}, \forall i \in \mathcal{V}. \tag{18}$$

Remark 3. *For any nodes j neighboring i where it holds that $\max_{j \in \mathcal{N}_i}\{V_{0j}\} > V_{0i}$, one can represent* (18) *as*

$$m_i^q \beta_i^q \leq K_i, \forall i \in \mathcal{V} \tag{19}$$

where we define

$$K_i := \frac{1}{2\left(\max_{j \in \mathcal{N}_i}\{V_{0j}\} - V_{0i}\right) |B_{ii}|}. \tag{20}$$

The term $m_i^q \beta_i^q$ represents the effective droop gain, as demonstrated in (5)*. Additionally, we can observe from* (20) *that the higher $|B_{ii}|$, the lower the value of $K(i)$.*

Proof. By treating our MIMO model as two SISO dynamical subsystems, the stability of the entire bus dynamics can be ensured by independently verifying the stability of each SISO system. After transforming our model from Fig. 1 to Fig. 3, we can consider the feedback loop as equivalent to Fig. 2 where G and $\frac{1}{s} L$ are given by (11). Suppose (18) is fulfilled, then **Lemma 1** implies that our network model $\frac{1}{s} L$ satisfies $0 \preceq L \preceq I$. Therefore, we can utilize **Theorem 1** to verify the stability.

Let g_i^V and g_i^θ describe the voltage magnitude and angle dynamics of bus i, respectively. We then can define

$$g_i^{\frac{V}{=}} \quad \frac{\gamma_i^q m_i^q \beta_i^q}{V_{0i} \tau_i^q}.$$

Since $g_i^V \geq 0$ for all i, then by **Theorem 1** we can easily choose any positive constant $f \in PR \cap \mathscr{A}_0$ such that $g^V \in \mathcal{G}_f$. We also have

$$g_i^{\frac{\theta}{=}} \quad \frac{\gamma_i^p m_i^p \beta_i^p}{V_{0i}(\tau_i^p s + 1)}.$$

Let $f(s) = \frac{s}{s+T}$ for some $T \in \mathbb{R}_{>0}$. Let

$$F := \frac{s}{s+T}\left(1 + \frac{\gamma_i^p m_i^p \beta_i^p}{s V_{0i}(\tau_i^p s + 1)}\right) - \epsilon.$$

We will show that for all i, there exists an $\epsilon > 0$ such that

$$F \in PR \tag{21}$$

and, thus, $g_i^\theta \in \mathcal{G}_f$. Simplifying the expression of F, we get

$$F = \frac{\xi_{2,i}s^2 + \xi_{1,i}s + \xi_{0,1}}{\eta_{2,i}s^2 + \eta_{1,i}s + \eta_{0,1}},$$

where $\xi_{2,i} := (1-\epsilon)\tau_i^q$, $\xi_{1,i} := 1-\epsilon-T\epsilon\tau_i^q$, $\xi_{0,i} := \gamma_i^p\, m_i^p \beta_i^p - T\epsilon$, $\eta_{2,i} := V_{0i}\tau_i^q$, $\eta_{0,i} := W_{0i}(T+\tau_i^q)$. We can choose T sufficiently large and ϵ small enough such that, for all i,

$$\left(\sqrt{\xi_{0,i}\eta_{2,i}} - \sqrt{\xi_{2,i}\eta_{0,i}}\right)^2 \leq \xi_{2,i}\eta_{0,i} \leq \xi_{1,i}\eta_{1,i},$$

from which the result (21) immediately follows [16, Cor. 11]. Therefore, satisfying (18) makes the feedback interconnection in Fig. 1 stable. □

IV. Numerical Illustration

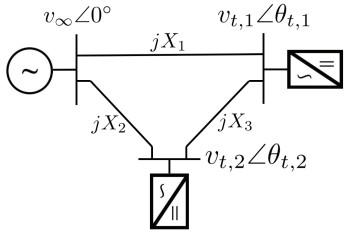

Figure 4. Three-bus power system.

Table I
Parameter values of the network

Parameter	Symbol	Value	Unit
Reactance	X_1, X_2, X_3	0.15, 0.20, 0.15	p.u.
Droop gain	m_1^p, m_2^p, m_1^q, m_2^q	0.05, 0.05, 0.05, 0.05	–
Filter gain	β_1^p, β_2^p	1, 1	–
Upper bound	K_1/m_1^q, K_2/m_2^q	0.75, 0.86	–
Time constant	τ_1^p, τ_2^p, τ_1^q, τ_2^q	50, 50, 50, 50	rad/s

We consider a three-bus system consisting of two GFM IBRs and an infinite bus in a network as shown in Fig. 4. Nominal parameter values of the system are given in Table I. We choose various operating points and DC gain β^q as listed in Table II, then use the small-disturbance (eigenvalue) analysis to analyze the stability around the equilibrium point under those values.

Table II
Simulation cases

Case	β_1^q, β_2^q	P_1^0, P_2^0	Q_1^0, Q_2^0	V_1^0, V_2^0
1	0.50, 0.50	1.0, 1.0	0.2, 0.2	1.0, 1.0
2	0.75, 0.75	1.0, 1.0	0.2, 0.2	1.0, 1.0
3	0.75, 0.75	0.8, 0.8	0.1, 0.1	0.9, 0.9

Eigenvalues of the linearized system are presented in Table III. It is noteworthy that meeting condition (18) results in eigenvalues with negative real parts in all cases, for all the chosen operating points. This implies stable dynamics around the equilibrium points.

Table III
Eigenvalues of the linearized system ($\times 10^4$)

Case 1	Case 2	Case 3
$-1.7934 + j0.0000$	$-2.6878 + j0.0000$	$-2.6326 + j0.0000$
$-0.7321 + j0.0000$	$-1.0962 + j0.0000$	$-1.0648 + j0.0000$
$-0.0025 + j0.2063$	$-0.0025 + j0.2063$	$-0.0025 + j0.1823$
$-0.0025 - j0.2063$	$-0.0025 - j0.2063$	$-0.0025 - j0.1823$
$-0.0027 + j0.1282$	$-0.0027 + j0.1282$	$-0.0026 + j0.1173$
$-0.0027 - j0.1282$	$-0.0027 - j0.1282$	$-0.0026 - j0.1173$

V. Conclusion

We present decentralized stability criteria for droop-controlled grid-forming inverters. Our approach involves analyzing the $Q-V$ coupling in the network Jacobian matrix and applying loop transformation for adjustments. The resulting criteria rely solely on properly tuning the droop gains of each local controller, as illustrated through numerical exam-ples. Future works include expanding our analysis on models with higher fidelity and incorporating heterogeneous grid-edge components, including grid-following IBRs.

References

[1] T. Ackermann, T. Prevost, V. Vittal, A. Roscoe, J. Matevosyan, and N. Miller, "Paving the way: A future without inertia is closer than you think," *IEEE Power and Energy Magazine*, vol. 15, no. 6, pp. 61–79, 2017.

[2] F. Milano, F. Dörfler, G. Hug, D. J. Hill, and G. Verbič, "Foundations and challenges of low-inertia systems," in *Power Systems Computation Conference (PSCC)*, 2018, pp. 1–25.

[3] "West murray zone sub-synchronous oscillations october 2022," Australian Energy Market Operator (AEMO), Tech. Rep., October 2022.

[4] S. Barsarkar and P. Kundur, "Hierarchical stability and alert state steering control of interconnected power systems," *IEEE Transactions on Circuits and systems*, vol. 27, no. 11, pp. 1102–1112, 1980.

[5] Y. Guo, D. Hill, and Y. Wang, "Global transient stability and voltage regulation for power systems," *IEEE Transactions on Power Systems*, vol. 16, no. 4, pp. 678–688, 2001.

[6] U. Markovic, O. Stanojev, P. Aristidou, E. Vrettos, D. Callaway, and G. Hug, "Understanding small-signal stability of low-inertia systems," *IEEE Transactions on Power Systems*, vol. 36, pp. 3997–4017, 2021.

[7] S. Geng and I. A. Hiskens, "Unified grid-forming/following inverter control," *IEEE Open Access Journal of Power and Energy*, vol. 9, pp. 489–500, 2022.

[8] S. Jafarpour, V. Purba, B. Johnson, S. Dhople, and F. Bullo, "Singular perturbation and small-signal stability for inverter networks," *IEEE Transactions on Control of Network Systems*, vol. 9, no. 2, pp. 979–992, June 2022.

[9] D. Pal, B. K. Panigrahi, B. Johnson, D. Venkatramanan, and S. Dhople, "Large-signal stability analysis of three-phase grid-following inverters," *IEEE Transactions on Energy Conversion*, pp. 1–15, 2023.

[10] Z. Wang, S. Mei, F. Liu, S. H. Low, and P. Yang, "Distributed load side control: Coping with variation of renewable generations," *Automatica*, vol. 109, pp. 1–14, 2019.

[11] H.-D. Chang, C.-C. Chu, and G. Cauley, "Direct stability analysis of electric power systems using energy functions: theory, applications, and perspective," *Proceedings of the IEEE*, vol. 83, no. 11, pp. 1497–1529, 1995.

[12] R. Pates and E. Mallada, "Robust scale-free synthesis for frequency control in power systems," *IEEE Transactions on Control of Network Systems*, vol. 6, no. 3, pp. 1174–1184, 2019.

[13] P. Kundur, *Power System Stability and Control, 2nd edition*. New York, USA: McGraw-Hill, 2022.

[14] S. Kundu, S. Geng, S. P. Nandanoori, I. A. Hiskens, and K. Kalsi, "Distributed barrier certificates for safe operation of inverter-based microgrids," in *2019 American Control Conference (ACC)*. IEEE, 2019, pp. 1042–1047.

[15] R. A. Horn and C. R. Johnson, *Topics in matrix analysis, 1991*. Cambridge, UK: Cambridge University Presss, 1991.

[16] M. Chen and M. Smith, "A note on tests for positive-real functions," *IEEE Transactions on Automatic Control*, vol. 54, pp. 390–393, 2009.